

THE THIRD VLBA CALIBRATOR SURVEY — VCS3

L. PETROV

NVI, Inc./NASA GSFC, Code 926, Greenbelt, MD 20771, USA

Y. Y. KOVALEV[†]

National Radio Astronomy Observatory, P.O. Box 2, Green Bank, WV 24944, USA; and
Astro Space Center of P.N. Lebedev Physical Institute, Profsoyuznaya 84/32, 117997 Moscow, Russia

E. FOMALONT

National Radio Astronomy Observatory, 520 Edgemont Road, Charlottesville, VA 22903–2475, USA

D. GORDON

Raytheon/NASA GSFC, Code 926, Greenbelt, MD 20771, USA

Submitted on September 28, 2004

ABSTRACT

This paper presents the third extension to the Very Large Baseline Array (VLBA) Calibrator Survey, containing 360 new sources not previously observed with very long baseline interferometry (VLBI). The survey, based on three 24 hour VLBA observing sessions, fills the areas on the sky above declination -45° where the calibrator density is less than one source within a 4° radius disk at any given direction. The positions were derived from astrometric analysis of the group delays determined at 2.3 and 8.4 GHz frequency bands using the Calc/Solve package. The VCS3 catalogue of source positions, plots of correlated flux density versus the length of projected baseline, contour plots and fits files of naturally weighted CLEAN images as well as calibrated visibility function files are available on the Web at <http://gemini.gsfc.nasa.gov/vcs3>

Subject headings: astrometry — reference frames — astronomical data bases: catalogues — quasars: general — radio continuum: general — reference systems: techniques — interferometric

1. INTRODUCTION

Catalogues of positions of compact radio sources with the highest precision are the basis for many applications. Among of them are imaging faint radio sources in phase referencing mode, monitoring the Earth's rotation, space geodesy, and space navigation. The method of VLBI first proposed by Matveenko et al. (1965) allows us to determine positions of sources with nanoradian precision ($1 \text{ nrad} \approx 0.2 \text{ mas}$). The first catalogue of source positions determined with VLBI (Cohen & Shaffer 1971) contained only 35 sources. It is desirable for the above mentioned applications to have many more sources. In 1998 the ICRF catalogue of 667 sources produced by analyzing VLBI observations made in the framework of space geodesy programs was published (Ma et al. 1998). Six years later, the extension of this catalogue, ICRF-Ext2, with 109 more sources, was published (Fey et al. 2004). However, the sky coverage of these catalogues is still not sufficient for some applications. Successful phase referencing requires having a calibrator within 4° from the target source with a precise position and known source structure. The probability of finding a calibrator from the ICRF-Ext2 catalogue within 4° of any random target above -45° declination is about 50%. Also, the ICRF catalogue does not provide source maps. In order to overcome these deficiencies, twelve 24 hour observing sessions with the VLBA, called VLBA Calibrator Surveys, were performed. Analysis of these obser-

vations produced the VCS1 (Beasley et al. 2002) and VCS2 (Fomalont et al. 2003) catalogues of 1611 new sources not listed in the ICRF catalogue. Approximately 80% of these sources are suitable as phase referencing calibrators and target sources for space geodesy programs.

Combining all suitable calibrators from the ICRF-Ext2, VCS1 and VCS2 catalogues we get a list of 1986 sources. Over 89.5% of the sky north of -45° declination we find at least one calibrator within a 4° radius disk at any given direction. In this paper we present an extension of the VCS1 and VCS2 catalogues, called the VCS3 catalogue, mainly concentrating on the other 10.5% of the sky where the source density is lowest. Since the observations, calibrations, astrometric solutions and imaging are close to that of VCS1, most of the details have been described by Beasley et al. (2002). In section 2 we describe the strategy for selection of 450 candidate sources observed in three 24 hour sessions with the VLBA. In section 3 we briefly outline the observations and data analysis. We present the catalogue in section 4, summarize our results and in section 5.

2. SOURCE SELECTION

Having unlimited resources one could try to observe all sources stronger than some limit. However, only sources with bright compact components can be detected with VLBI and might be useful for phase referencing or geodetic applications. Kellermann, Pauliny-Toth, & Davis (1968) first showed that the distribution of sources over spectral index α ($F \propto \nu^\alpha$) has two peaks: one near $\alpha = -1$ (steep spectrum) and another near 0 (flat spectrum). Later, it was confirmed that extended objects dominate in the steep spectrum popula-

Electronic address: Leonid.Petrov@lpetrov.net
Electronic address: ykovalev@nrao.edu
Electronic address: efomalont@nrao.edu
Electronic address: dgg@leo.gsfc.nasa.gov

[†] Karl Jansky Fellow

tion (see the review by Kellermann & Owen 1988). In compact regions, which have the synchrotron mechanism of emission, the peak in the spectrum caused by synchrotron self-absorption has frequencies higher than 1 GHz due to their small size. Thus, if a dominating source of emission comes from compact regions, the spectrum of the total flux density will be predominantly flat or inverted.

Examining spectral indexes of the PKScat90 catalogue (Wright and Otrupcek 1990), which is believed to be complete at the 95% level for sources with flux density > 0.25 Jy at 2.7 GHz (Bolton, Savage, & Wright 1971), we found that only 26% of sources have spectral indexes > -0.5 . Myers et al. (2003) used NVSS (Condon et al. 1998) and GB6 (Gregory et al. 1996) catalogues for selection of sources with spectral indexes > -0.5 at 5 GHz, and they found 11685 sources brighter than 30 mJy level, or 24% of the total number of sources. It should be noted that a significant fraction of the sources with spectral index in the range $[-0.5, -0.4]$ belongs to the steep spectrum population and are expected to have extended structure. Thus, taking sources at random, the probability that a source will be compact, and therefore, detectable with VLBI does not exceed 20%. A carefully designed strategy for source selection can significantly increase the yield of detections.

We considered all bright sources at X-band (8.4 GHz) and S-band (2.3 GHz) with spectral indexes greater than -0.5 as candidates for the VCS3 campaign. In order to find these sources, we first analyzed catalogues of compact flat-spectrum sources: JVAS (Wrobel et al. 1998), CLASS (Myers et al. 2003), Parkes quarter-Jansky catalogue (Jackson et al. 2002), VLA South (Winn, Patnaik, & Wrobel 2003) and selected all sources brighter than 100 mJy at declinations above -45° with arc distances from any known calibrator greater than 3.9° . This produced a list of 374 sources. Not all these catalogues provide flux density at more than one band. We used the CATS database (Verkhodanov et al. 1997) for cross-checking the reported flux density and for acquiring information about flux measurements for these objects from other sources. Unfortunately, most of these measurements were done at different epochs. Since many flat spectrum sources are variable, the estimates of the spectral index made at different epochs may be unreliable. Instantaneous 1–22 GHz broad-band spectra for 3000 AGN with flux density greater than 100 mJy at 13 cm and $\alpha > -0.5$, including many sources from this list, were observed with the Russian 600 meter ring radio telescope RATAN–600 in transit mode (see method of observations and data reduction in Kovalev et al. 1999) as a part of an ongoing survey program. Those flat spectrum sources from this sample which have flux density greater than 200 mJy at X and/or S band and have not been previously observed with VLBI, in total, 116 sources, were included in the VCS3 candidates list. After cross checking we removed sources from the list for which the estimate of the spectral index was either unreliable or less than -0.5 . The total number of sources selected from these catalogues was 300.

After picking up these 300 sources from all known compact flat-spectrum catalogues we still had areas where the density of calibrators was less than the targeted density. In order to fill these areas we used the NVSS catalogue of about 1.8 million sources (Condon et al. 1998). First, we selected 2704 sources with total flux density greater than 100 mJy at 1.4 GHz in the areas where the distance to the closest calibrator and already selected candidates was greater than 4° . However, the NVSS catalogue does not provide information

about spectral index. We checked these 2704 sources against the CATS database, which contains almost all available radio catalogues, and found the sources observed under other campaigns at different frequency bands. If they were not found in any other catalogue, for example, they were absent in the GB6 catalogue with flux limit 18 mJy and in the PMN (Wright et al. 1996) catalogue with flux limit 40–70 mJy at 5 GHz, this indicates that with a high probability their spectral index is significantly less than -0.5 . In total, this initial list had 302 sources.

We examined the spectrum provided by CATS and subjectively ascribed a class to each source:

- 0 — the source has flat spectrum, and the estimate of the spectral index is reliable (e.g., RATAN–600 instantaneous spectrum is available), and the estimated correlated flux density is greater than 100 mJy;
- 1 — the estimate of the spectral index is less reliable, or the spectral index is in the range $[-0.4, -0.2]$, and the estimated correlated flux density is greater than 100 mJy;
- 2 — the estimate of the spectral index is unreliable or in the range of $[-0.5, -0.4]$, and/or the estimated correlated flux density is less than 100 mJy.

Then for each source we computed a score based on angular distance to the closest calibrator, flux density, spectral index and class:

$$S = 10^3 ((D - D_{lim}) / D_{lim})^3 + 10^5 (\alpha + 0.5)^3 + 2 \cdot 10^2 (2 - C) + \lg F \quad (1)$$

where D — angular distance to the closest calibrator or already selected candidate, D_{lim} minimal angular distance (4°), α — spectral index, C — class, F — flux density in Jy extrapolated to 8.4 GHz. An iterative procedure computed the score, selected the source with the largest score and ran again. Using this method we picked up 150 sources with the highest score in addition to the 300 sources previously chosen.

3. OBSERVATIONS AND DATA ANALYSIS

The VCS3 observations were carried out in three 24 hour observing sessions with the VLBA on 2004 April 30, 2004 May 08, and 2004 May 27. Since the correlated flux density for selected candidates was expected to be different, we split our sources into three categories:

- a — sources of class 0 brighter than 200 mJy;
- b — sources of class 0 with flux density in the range 100–200 mJy or sources of class 1 brighter than 200 mJy;
- c — all other sources.

Integration time was chosen to be 90 seconds for sources from category a, 180 seconds from category b, and 300 seconds from category c. The sources above -20° declination were scheduled for two scans at different hour angles in order to improve the uv coverage. The target sources were observed in a sequence designed to minimize loss of time from antenna slewing. In addition to the target sources, 77 strong sources were taken from the Goddard astrometric and geodetic catalogue 2004a_astro². Observations of 3–4 strong sources from

² <http://gemini.gsfc.nasa.gov/solutions/astro>

this list were made every 1–1.5 hours during observing sessions. These observations were scheduled in such a way, that at each station at least one of these sources was observed at an elevation angle less than 20° , and at least one source was observed at an elevation angle greater than 50° . The purpose of these observations was to provide calibration for mismodelled troposphere path delays and to tie the VCS3 source positions to the ICRF catalogue. On average, the antennas were on-source 70% of the time.

The observations used the VLBA dual-frequency geodetic mode, observing simultaneously at 2.3 GHz and 8.4 GHz. Each band was separated into four 8 MHz channels (IFs) which spanned 140 MHz at 2.3 GHz and 490 MHz at 8.4 GHz, in order to provide precise measurements of group delays for astrometric processing. Since the a priori coordinates of many candidates were expected to have errors of up to $30''$, the data were correlated with an accumulation period of 1 second in 64 frequency channels in order to provide extra-wide windows for fringe searching.

Processing of the VLBA correlator output to obtain the astrometric observables was made using the Astronomical Image Processing System (AIPS) (Greisen 1988). The data was first phase calibrated using the measured phase cal phases for each scan and each channel. Then the phases of a single strong calibrator scan were subtracted from each scan to flatten out the phases across the band of each individual channel. Sampler bias correction together with initial amplitude calibration was performed using the recorded system temperatures and gain tables (tasks “ACCOR” and “APCAL”). Task “FRING” was then run for each baseline separately (with SNR cutoff = 3) to obtain the residual narrow-band group delays for each channel, residual single channel fringe phases, and residual single channel phase delay rates. Task “MBDLY” was then used to compute the residual group delays from the 4 single channel fringe phases at each frequency band. Then task “CL2HF” was used to compute the total group delays, phase delay rates and fringe phases by combining the residuals with the correlator model, and converting them from geocenter to reference station quantities. Finally, the AIPS output was reformatted for input into the Calc/Solve geodetic/astrometric VLBI analysis software package³ using task “HF2SV”.

The software package Calc/Solve was used for determination of accurate positions of all detected sources. Astrometric analysis was performed in several steps. First, we used narrow-band group delays determined over each 8 MHz wide channel and incoherently separately over all channels within X and S band. Narrow-band group delays are less precise than wide-band group delay data, but they have very wide ambiguity spacings: 4 mks. In the first step X-band single-band delay data (and S-band data for the sources detected only at S-band) were used for estimation of new source positions and clock functions modeled by a second degree polynomial. These estimates were used in an S-band wide-band group delay solution for short baselines between stations Pietown, Kitt Peak, Owens Valley, Los Alamos and Fort Davis in order to resolve the group delay ambiguities which had spacings of 100 ns. In the second step after resolving ambiguities, these data were used for source position determination. In the step three these estimates were used in an S-band group delay solution for longer baselines for further ambiguity resolution. In the fourth step the previous estimates of source positions were

used for ambiguity resolution of X-band group delays (with spacings 29 ns) on short baselines, and a new solution was made. These estimates then were used for resolving X-band group delays at long baselines in the next step. In the sixth step ionosphere free combinations of X and S band wide-band group delays were used for data analysis. The estimation model at this step included coefficients of linear splines for clocks of all stations, except a reference station, and troposphere zenith path delay at all sites. The time interval for linear splines was 60 minutes. The data were carefully analyzed for the presence of any remaining errors in group delay ambiguity resolution and for outliers. About 1% of the data were deselected, primarily because the fringe fitting algorithm picked a secondary maximum of the delay resolution function. If only two observations of a source are used in a solution, errors in group delay ambiguity resolution cannot be detected. However, if more observations are used in a solution, errors in group delay ambiguity resolution can result in a significant misfit. Therefore, analysis of observations of sources with numerous misfits allowed us to detect group delay ambiguity resolution errors when at least 3–6 observations. Being conservative, we set to 8 the minimum number of observations needed in order to rule out the possibility of group delay ambiguity resolution errors. After outlier elimination we determined additive baseline-dependent corrections to the a priori weights in such a manner that the ratios of the sums of weighted squares of post-fit residuals to their mathematical expectation are close to unity.

In the final solution all available astrometric and geodetic data from August 1979 to August 2004, including the three VCS3 sessions, were used in a single least square solution. Estimated parameters included positions and velocities of stations, coordinates of all sources, Earth orientation parameters, clock functions and troposphere zenith path delays. The only differences in treatment of the VCS3 sessions with respect to other experiments were that we did not estimate troposphere gradients and the time interval for clocks and troposphere zenith path delays were 60 minutes instead of 20 minutes. Since a few sources were detected in only one band, we made three solutions: using 1) ionosphere free linear combinations of X-band and S-band wide-band group delays, 2) only X-band group delays and 3) only S-band group delays.

Since the equation for time delay is invariant with respect to the group of coordinate transformations, observations themselves do not determine source positions, but only a family of positions. In order to pick a specific element of this family, we imposed boundary conditions by applying net-rotation constraints on the positions of 212 sources listed as “defined” in the ICRF catalogue such that the set of new positions of these 212 sources did not have a net-rotation with respect to the set of old position from the ICRF. More details about this procedure can be found in Beasley et al. (2002).

In order to evaluate position errors we made a special solution using only the three VCS3 sessions in which we estimated coordinates of all sources and applied no-net-rotation constraints on 20 sources common in the VCS3 and ICRF defining lists. Since 77 sources used in the VCS3 campaign were intensively observed earlier under various geodetic and astrometric programs, we used the differences between very accurate positions derived from analysis of these observations and positions from the VCS3 sessions as a measure of the upper limit of VCS3 catalogue errors. We represent estimates of errors in right ascension (σ_α) and in declination (σ_δ) of the

³ <http://gemini.gsfc.nasa.gov/solve>

TABLE 1
ADDITIVE CORRECTIONS TO FORMAL UNCERTAINTIES APPLIED FOR DERIVATION OF ERRORS
OF SOURCE POSITION IN VCS3 CATALOGUE

Declination zone (deg)	X/S			X-band			S-band		
	# pts	E_α (mas)	E_δ (mas)	# pts	E_α (mas)	E_δ (mas)	# pts	E_α (mas)	E_δ (mas)
(+20.0, +90.0)	33	0.2	0.4	96	0.6	0.5	94	5.1	4.7
(0.0, +20.0)	16	0.3	0.2	77	0.5	0.6	77	4.2	7.2
(-20.0, 0.0)	11	0.2	0.3	64	0.8	1.5	64	7.0	16.8
(-30.0, -20.0)	11	0.2	0.7	44	1.2	1.8	44	13.0	27.6
(-45.0, -30.0)	13	0.3	0.4	76	2.4	7.3	75	40.0	40.0

VCS3 catalogue in the form:

$$\sigma_\alpha = \sqrt{(1.5 \cdot \sigma_\alpha^r)^2 + E_\alpha^2(\delta) / \cos^2 \delta}$$

$$\sigma_\delta = \sqrt{(1.5 \cdot \sigma_\delta^r)^2 + E_\delta^2(\delta)}$$
(2)

where σ_α^r and σ_δ^r stand for the formal uncertainties derived by the errors propagation law from fringe amplitude signal to noise ratios, E_α and E_δ are additive reweighting parameters. The multiplicative factor 1.5 in (2), first found by Ryan et al. (1993), accounts underestimated systematic errors in computation of uncertainties of wide-band group delays and affects uncertainties of estimates of all parameters from VLBI, including source coordinates. We split the sources into five declination zones, and for each group we found the values of E_α and E_δ which made ratios of weighted sum of squares of residuals to its mathematical expectation close to unity. Using this techniques we computed additive corrections to uncertainties of the estimates of X-band only and S-band only solutions by analyzing the differences between dual band and single band solutions. Reweighting parameters are presented in Table 1. The histogram of source position errors is presented in Figure 1.

For imaging purpose the data were re-processed with the global fringe fitting procedure (task “FRING”) with SNR cutoff 4 at each individual channel. Global, station-based

fringing allows detection of weaker sources than the baseline-based fringing used for astrometric analysis. (We did not use global fringing for astrometric analysis, since as we found earlier, it gives less reliable group delays than baseline-based fringing). A bandpass correction was then determined with the task “BPASS”. After initial editing the fringe amplitude and phases were averaged across the channels. We used the AIPS task “CALIB” in order to perform the first step of the self-calibration procedure applying the point source model. The whole scan length was used to find the combined solution for the channels with the SNR cutoff 3. After that we imported data to the Caltech DIFMAP package (Shepherd 1997). We have adapted the automated procedure originally written by by Greg Taylor (Pearson et al. 1994) for self-calibration and imaging of the VCS3 short snapshot observations.

For each detected source at each band, we have computed two estimates of correlated flux density: one averaged over the entire image (total CLEAN flux density) and another averaged only over the spatial frequencies in the range [0.8, 1.0] of the maximum spatial frequencies. The latter estimate characterizes the flux density of unresolved components. Errors of our estimates of total correlated flux density of sources brighter than 100 mJy are determined mainly by the accuracy of amplitude calibration, which for the VLBA, according to Wrobel and Ulvestad (2004), is at the level of 5% at 1–10 GHz. This estimate was confirmed by the comparison of the correlated flux density with the single-dish flux density measured with RATAN–600 in October 2003 for several slowly varying sources without extended structure. The contribution of fringe amplitude errors is significant for sources with flux density < 100 mJy. The error of correlated flux density for this group of sources is about 10%. It should be noted that in the case of a source with asymmetric extended structure the estimate of the correlated flux density from unresolved components may be biased due to a significant non-uniformity of uv coverage at long spacings.

In total, 365 out of 450 sources were detected and yielded at least two good points for position determination. However, not all of these sources are suitable as phase referencing calibrators or as targets for geodetic observations. We consider a source suitable as a calibrator if 1) the number of good X/S pairs of observations is 8 or greater in order to rule out the possibility of a group delay ambiguity resolution error; and 2) position error before reweighting is less than 5 mas. We found that usually 8 observations at the VLBA is sufficient to get positions with errors less than 5 mas. If the errors are significantly greater, this means that the source was not detected at long baselines, and therefore, we do not possess information whether on the source can be detected when used as a phase referencing calibrator. Only 231 sources satisfy this

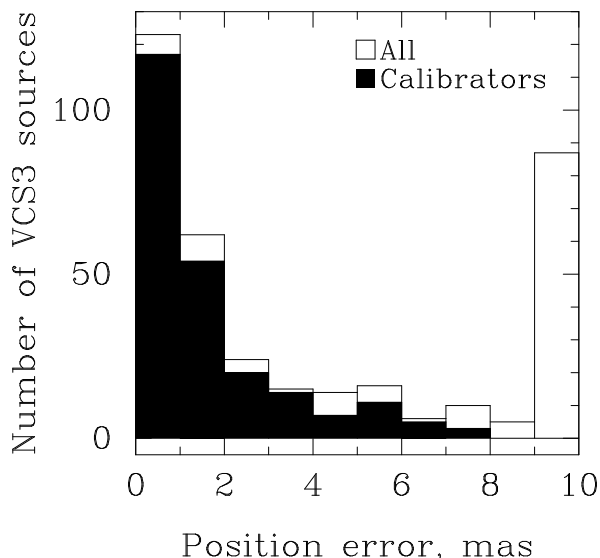


FIG. 1.— Histogram of semi-major error ellipse of position errors. The last bin shows errors exceeding 9 mas.

TABLE 2
THE VCS3 CATALOGUE

Cls (1)	Source name		J2000.0 Coordinates		Errors (mas)			# Obs (9)	Correlated flux density (Jy)				Band (14)
	IVS (2)	IAU (3)	Right ascension (4)	Declination (5)	$\Delta\alpha$ (6)	$\Delta\delta$ (7)	Corr (8)		X-band		S-band		
C	0001-120	J0004-1148	00 04 04.914997	-11 48 58.38564	0.24	0.40	-0.069	20	0.42	< 0.11	0.81	< 0.06	X/S
-	0003+340	J0006+3422	00 06 07.382435	+34 22 20.41138	1.83	4.46	-0.233	5	< 0.06	< 0.06	< 0.06	< 0.06	X
C	0009+655	J0012+6551	00 12 37.671095	+65 51 10.82363	9.21	4.00	0.040	10	0.10	0.09	0.47	0.10	X/S
-	0017+296	J0019+2956	00 19 37.791440	+29 56 01.93471	19.34	7.63	-0.015	14	< 0.06	< 0.06	< 0.06	< 0.06	S
-	0021-084	J0024-0811	00 24 00.672740	-08 11 10.04935	4.75	8.88	-0.010	15	< 0.07	< 0.06	0.08	< 0.06	X
C	0026-015	J0029-0113	00 29 00.986049	-01 13 41.76047	0.74	0.95	0.349	36	0.19	< 0.06	0.17	0.08	X/S
C	0027-024	J0030-0211	00 30 31.823755	-02 11 56.13361	0.30	0.57	-0.243	68	0.26	0.18	0.12	0.09	X/S
C	0029-147	J0031-1426	00 31 56.411853	-14 26 19.34670	0.93	1.60	-0.607	36	0.12	< 0.06	0.24	0.12	X/S
C	0042+186	J0044+1855	00 44 42.227898	+18 55 05.03460	0.76	1.69	0.591	36	0.08	< 0.06	0.14	0.10	X/S
-	0042-373	J0045-3705	00 45 12.065955	-37 05 48.47087	3.05	7.43	-0.066	20	0.17	0.13	0.09	0.10	X
C	0043+246	J0046+2456	00 46 07.825737	+24 56 32.52438	0.26	0.46	0.051	90	0.43	0.33	0.18	0.14	X/S
C	0046+063	J0048+0640	00 48 58.723150	+06 40 06.47544	0.67	1.20	0.414	28	0.12	< 0.06	0.25	0.07	X/S
C	0054+161	J0056+1625	00 56 55.294324	+16 25 13.34088	0.33	0.29	0.019	90	0.43	0.40	0.28	0.27	X/S
C	0055+060	J0058+0620	00 58 33.804542	+06 20 06.07296	0.68	1.31	-0.047	81	0.17	0.15	< 0.06	< 0.06	X

NOTE. — Table 2 is presented in its entirety in the electronic edition of the *Astronomical Journal*. A portion is shown here for guidance regarding its form and contents. Units of right ascension are hours, minutes and seconds, units of declination are degrees, minutes and seconds

calibrator criteria. It should be mentioned that our criterion for suitability of using a source as a phase calibrator is rather conservative, and the sources which fail this criterion may still be useful for some applications.

Five detected sources turned out to be known gravitational lenses. Since the fringe amplitude may have several minima and maxima during integration time for such sources, our technique for fringe searching is not applicable. We excluded gravitational lenses from the analysis, since they are, certainly, not suitable as calibrators.

4. THE VCS3 CATALOGUE

The VCS3 catalogue is listed in Table 2. The first column gives source class: “C” if the source can be used as a calibrator, “-” if it cannot. The second and third columns give IVS source name (B1950 notation), and IAU name (J2000 notation). The fourth and fifth columns give source coordinates at the J2000.0 epoch. Columns /6/ and /7/ give inflated source position uncertainties in right ascension and declination in mas, and the column /8/ gives the correlation coefficient between the errors in right ascension and declination. The number of group delays used for position determination is listed in column /9/. The next two columns give the estimates of correlated flux density at X-band: total CLEAN flux density (column /10/) and flux density of unresolved components (column /11/). Similar information for S-band is listed in columns /12/ and /13/. Column /14/ gives the code of observables used for position estimation: X/S stands for ionosphere-free linear combination of X and S wide-band group delays, X stands for X-band only group delays; S stands for S-band only group delays. Some sources which yielded less than 8 pairs of X and S band group delay observables had 2 or more observations at X and/or S band observations. For these sources either X-band only or S-band only estimates of coordinates are listed in the VCS3 catalogue, whichever uncertainty is less.

In addition to this table, the html version of this catalogue is posted on the Web at <http://gemini.gsfc.nasa.gov/vcs3>. For each source it has 8 links: to a pair of postscript maps of the source at X and S-band; to a pair of plots of cor-

related fringe amplitude as a function of the length of the baseline projection to the source plane; to a pair of fits files with CLEAN components of naturally weighted source images; to a pair of fits files with calibrated uv data. The coordinates and the plots are also accessible from the NRAO VLBA Calibration Search web-page http://magnolia.nrao.edu/vlba_calib/.

A sample of data used for candidate selection as well as some imaging results are shown in figure 2. In row /a/ we present the broad-band spectra from RATAN-600 observations in 2003 and from some old data taken from the NVSS, 87GB (Gregory & Condon 1991) and the Radio Survey of the Galactic Plane at 11cm (Fürst et al. 1990) catalogues. In rows /b/ and /d/ the dependence of visibility function amplitude versus projected baseline at S and X bands, respectively, is shown. Each point at the plots is a coherent average over the scan length. Naturally weighted CLEAN images at S and X bands are presented in rows /c/ and /e/.⁴ The sources in this figure are placed such that the contribution of the compact component in total emission increases from left to right. According to Kovalev et al. (2002), we interpret the broad-band spectrum as a sum of two constituents: emission from an optically thin extended component with steep spectrum which usually increases with decreasing the frequency up to hundreds MHz, and emission from a compact component with self-absorption which has a maximum at the frequency higher than 1 GHz. See discussion of compact steep spectrum sources in O’Dea (1998) for more details. The spectrum of J0012+6551 has the spectral index -0.5 . No contribution to emission from the compact component is seen, and the correlated flux density even at the shortest baseline projections is several times less than the total flux density. The source is below the detection limit at both bands at spacings $> 20 M\lambda$. At the X-band the map shows only noise. The spectrum of J0909+4253 has the spectral index -1.1 at frequencies less than 2 GHz and it flattens at higher frequencies. This flattening is caused by the contribution of the compact component. When the contribution of the extended compo-

⁴ The scale of the J0012+6551 map is increased with respect to other maps.

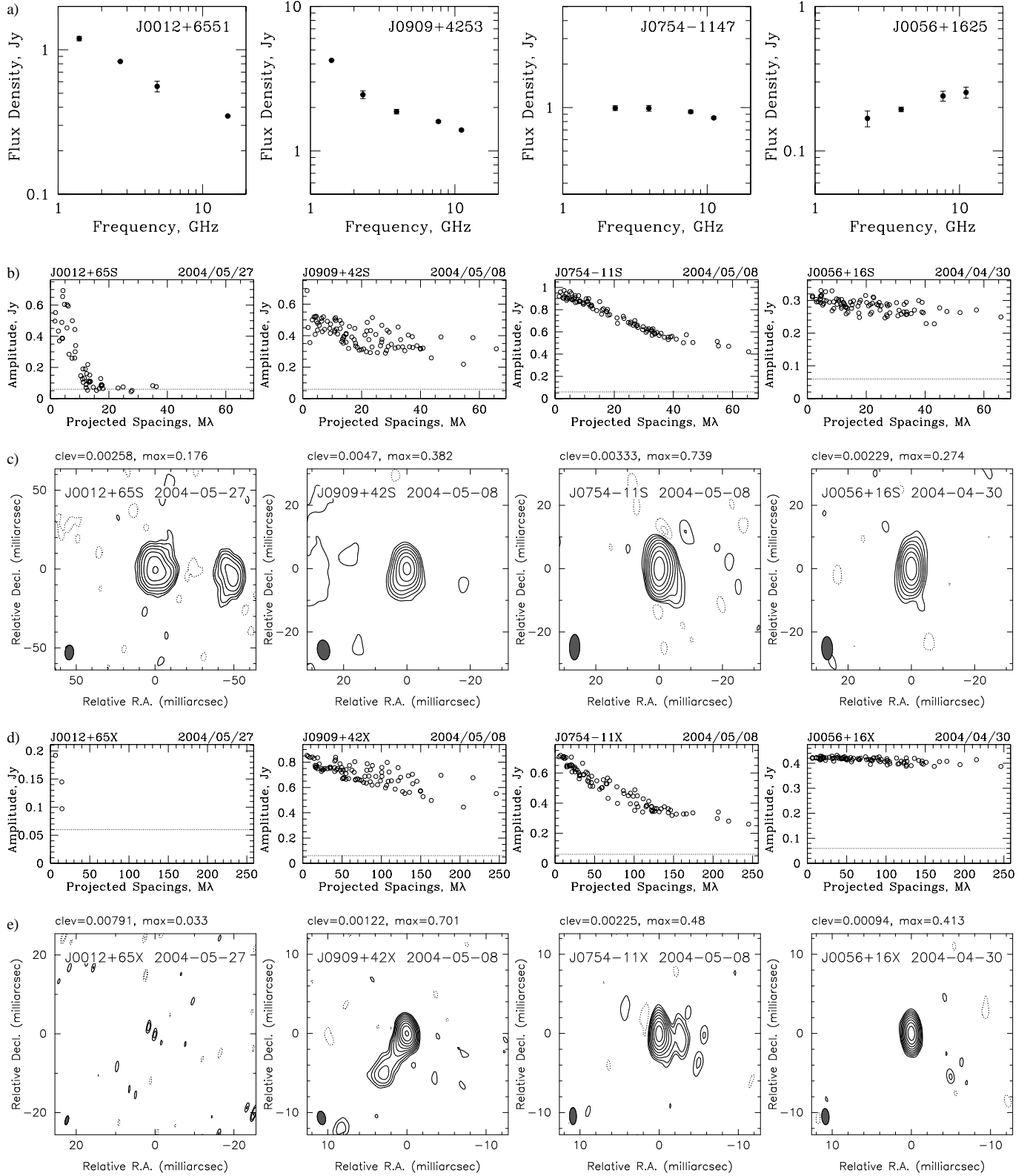


FIG. 2.— a) Broad-band spectra from RATAN-600 observations in 2003 plus data from CATS; b) dependence of the correlated flux density at S band versus projected spacings. A dot line shows the detection limit; c) naturally weighted CLEAN images at S bands. The lowest contour levels (2 steps) on images are plotted at “*clev*” levels [Jy/beam], the peak brightness — “*max*” values [Jy/beam]. The dashed contours indicate negative flux. The beam is shown in the bottom left corner of the images; d) dependence of the correlated flux density at X band versus projected spacings. e) naturally weighted CLEAN images at X bands.

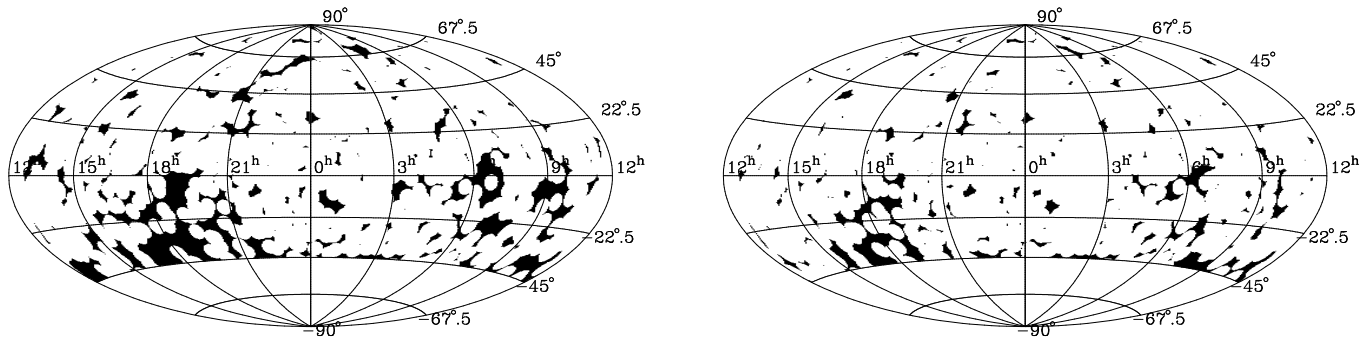


FIG. 3.— Source sky density before (left) and after (right) the VCS3 observing campaign. The area above -45° declination with calibrator source density less than one source within a 4° radius disk is shown in black.

ment is subtracted from the spectrum, the residual spectrum grows with an increase of the frequency, and our measurements of the correlated flux density confirm it. The remaining two sources have the flat and inverted spectra, which is an indication of a dominance of the compact constituent in total emission. Again our VLBA observations confirm it. Analysis of this sample illustrates the validity of our approach for candidate selection.

5. CONCLUSION

The VCS3 Survey has added 360 new sources which were previously not observed with VLBI. Of these, 231 sources are suitable as phase referencing calibrators and as target sources for geodetic applications. The careful strategy for source selection resulted in a very high detection rate; more than 80% of the sources in our candidates list were detected.

This campaign contributed considerably in reducing the areas with low density of known calibrators. If only sources from the ICRF-Ext2 catalogue are taken into account, 48.1% of the sky area above declination -45° has no calibrator within a 4° radius disk at any given direction. Combining the ICRF-Ext2 and the VCS1 catalogues, this area is reduced to 13.7%. Adding the VCS2 catalogue reduces the area to 10.5%. After the VCS3 campaign this area is only 5.3% of

the sky above declination -45° . Figure 3 shows the area with insufficient calibrators density before and after the VCS3 observing campaign.

The VLBA is a facility of the National Radio Astronomy Observatory which is operated by Associated Universities, Inc., under a cooperative agreement with the National Science Foundation. The authors made use of the database CATS (Verkhodanov et al. 1997) of the Special Astrophysical Observatory. This research has made use of the NASA/IPAC Extragalactic Database (NED) which is operated by the Jet Propulsion Laboratory, California Institute of Technology, under contract with the National Aeronautics and Space Administration. RATAN-600 observations were partly supported by the Russian State Program “Astronomy” and the Russian Ministry of Education and Science, the NASA JURRIS Program (project W-19611), and the Russian Foundation for Basic Research (01-02-16812 and 02-02-16305). The authors are thankful to D. McMillan for valuable comments. This work was done while L. Petrov and D. Gordon worked for NVI, Inc. and Raytheon, respectively, under NASA contract NAS5-01127.

REFERENCES

- Beasley, A. J., Gordon, D., Peck, A. B., Petrov, L., MacMillan, D. S., Fomalont, E. B., & Ma, C. 2002, *ApJS*, 141, 13
- Bolton, J. G., Savage, A., & Wright, A. E. 1979, *Australian Journal of Physics*, *Astroph. Suppl.*, 46, 1
- Cohen, M. H. & Shaffer, D. B. 1971, *AJ*, 76, 91.
- Condon, J. J., Cotton, W. D., Greisen, E. W., Yin, Q. F., Perley, R. A., Taylor, G. B., Broderick, J. J. 1998, *AJ*, 115, 1693
- Fey, A. L., Ma, C., Arias, E. F., Charlot, P., Feissel-Vernier, M., Gontier, A.-M., Jacobs, C. S., Li, J., MacMillan, D. S. 2004, *AJ*, 127, 3587.
- Fomalont E., Petrov, L., McMillan, D. S., Gordon, D., Ma, C. 2003, *AJ*, 126, 2562
- Fürst, E., Reich, W., Reich, P., & Reif, K. 1990, *A&AS*, 85, 805
- Gregory, P. C., & Condon, J. J. 1991, *ApJS*, 75, 1011
- Gregory, P. C., Scott, W. K., Douglas, K., & Condon, J. J. 1996, *ApJS*, 103, 427
- Jackson, C. A., Wall, J. V., Shaver, P. A., Kellermann, K. I., Hook, I. M., & Hawkins, M. R. S. 2002, *A&A*, 386, 97
- Kellermann, K. I., Pauliny-Toth, I. I. K., & Davis, M. M. 1968, *Astrophysical Letters*, 2, 105
- Kellermann, K. I. & Owen, F. N. 1988, *Galactic and Extragalactic Radio Astronomy*, ed. by G. L. Verschur & K. I. Kellermann (Springer Verlag), 563
- Kovalev, Y. Y., Nizhelsky, N. A., Kovalev, Yu. A., Berlin, A. B., Zhekanis, G. V., Mingaliev, M. G., & Bogdantsov, A. V. 1999, *A&AS*, 139, 545
- Kovalev, Y. Y., Kovalev, Yu. A., Nizhelsky, N. A., & Bogdantsov, A. B. 2002, *PASA*, 19, 83
- Ma, C. et al. 1998, *AJ*, 116, 516
- Matveenko, L. I., Karadashev, A. C., Sholomitskij, G. B., 1965, *Izvestia VUZov. Radiofizika*, 8, 651 (in Russian)
- Greisen, E. W., 1988, in *Acquisition, Processing and Archiving of Astronomical Images*, ed. G. Longo & G. Sedmak (Napoli: Osservatorio Astronomico di Capodimonte), 125
- Myers, S. T., et al., 2003, *MNRAS*, 341, 1
- O’Dea, C. P. 1998, *PASP*, 110, 493
- Pearson, T. J., Shepherd, M. C., Taylor, G. B., & Myers, S. T. 1994, *BAAS*, 185, 0808
- Ryan, J. W., Clark, T. A., Ma, C., Gordon, D., Caprette, D. S., & Himwich, W. E. 1993, *Global scale tectonic plate motions measured by CDP VLBI data*, 23, ed. by Smith, D. E. and Turcotte, D. L. (Washington, D.C.: American Geophysical Union, *Geodynamics Series*), 37
- Shepherd, M. C. 1997, in *ASP Conf. Series*, 125, *Astronomical Data Analysis Software and Systems VI*, ed. by G. Hunt & H. E. Payne (San Francisco: ASP), 77
- Verkhodanov, O. V., Trushkin, S. A., Andernach, H., & Chernenkov, V. N. 1997, in *ASP Conf. Ser.* 125, *Astronomical Data Analysis Software and Systems VI*, ed. G. Hunt, & H. E. Payne (San Francisco: ASP), 322
- Winn, J. N., Patnaik, A. R., & Wrobel, J. M. 2003, *ApJS*, 145, 83
- Wright, A. E. & Otrupcek, R. 1990, *Australia Telescope National Facility*, CSIRO, Parkes
- Wright, A. E., Griffith, M. R., Hunt, A. J., Troup E., Burke B. F., & Ekers R. D. 1996, *ApJS*, 103, 145
- Wrobel, J. M., Patnaik, A. R., Browne, I. W. A., & Wilkinson, P. N. 1998, *A&AS*, 193, 4004
- Wrobel, J. M. & Ulvestad, J. S. 2004, *VLBA status summary*, NRAO